Article

Development of Notch-Free, Pre-Bent Rod Applicable for Posterior Corrective Surgery of Thoracolumbar/Lumbar Adolescent Idiopathic Scoliosis

Yoko Ishikawa [1,2], Satoshi Kanai [3], Katsuro Ura [1], Terufumi Kokabu [1,2], Katsuhisa Yamada [1], Yuichiro Abe [2], Hiroyuki Tachi [1,2], Hisataka Suzuki [1,2], Takashi Ohnishi [1], Tsutomu Endo [1], Daisuke Ukeba [1], Masahiko Takahata [1], Norimasa Iwasaki [1] and Hideki Sudo [1,4,*]

1   Department of Orthopaedic Surgery, Hokkaido University Hospital, N15W7, Sapporo 060-8638, Hokkaido, Japan;
    y.ishikawa1105@gmail.com (Y.I.); notechoper@yahoo.co.jp (K.U.); m990015jp@yahoo.ne.jp (T.K.);
    yka2q@pop.med.hokudai.ac.jp (K.Y.); hitachi198885@gmail.com (H.T.); pingre_ya.4@icloud.com (H.S.);
    takashi.onishi.ortho@gmail.com (T.O.); m000053a@yahoo.co.jp (T.E.); daisuke922@nifty.com (D.U.);
    takamasa@med.hokudai.ac.jp (M.T.); niwasaki@med.hokudai.ac.jp (N.I.)
2   Department of Orthopaedic Surgery, Eniwa Hospital, 2-1-1 Kogane-Chuo, Eniwa 061-1449, Hokkaido, Japan;
    menchixp@gmail.com
3   Division of Systems Science and Informatics, Hokkaido University Graduate School of Information Science
    and Technology, N14W9, Sapporo 060-0814, Hokkaido, Japan
4   Department of Advanced Medicine for Spine and Spinal Cord Disorders, Faculty of Medicine,
    Graduate School of Medicine, Hokkaido University, N15W7, Sapporo 060-8638, Hokkaido, Japan
*   Correspondence: hidekisudo@yahoo.co.jp; Tel.: +81-11-706-5934

Abstract: Adolescent idiopathic scoliosis (AIS), the most common pediatric musculoskeletal disorder, causes a three-dimensional spine deformity. Lenke type 5 AIS is defined as a structural thoracolumbar/lumbar curve with nonstructural thoracic curves. Although a rod curvature will affect clinical outcomes, intraoperative contouring of the straight rod depends on the surgeon's knowledge and experience. This study aimed to determine the optimum rod geometries to provide a pre-bent rod system for posterior spinal surgery in patients with Lenke type 5 AIS. These pre-bent rods will be beneficial for achieving proper postoperative outcomes without rod contouring based on surgeon experience. We investigated 20 rod geometries traced in posterior spinal reconstruction in patients with Lenke type 5 AIS. The differences between the center point clouds in each cluster were evaluated using the iterative closest point (ICP) method with modification. Before the evaluation using the ICP method, the point clouds were divided into four clusters based on the rod length using a hierarchical cluster analysis. Because the differences in the values derived from the ICP method were <5 mm for each length-based cluster, four representative rod shapes were generated from the length-based clusters. We identified four optimized rod shapes that will reduce operation time, leading to a decreased patient and surgeon burden.

Keywords: adolescent idiopathic scoliosis; thoracolumbar/lumbar curve; pre-bent rod; iterative closest point method

1. Introduction

Adolescent idiopathic scoliosis (AIS) is a disorder that causes three-dimensional deformities of the pediatric spine [1,2]. Lenke et al. suggested a classification for AIS with six curve types, considering the lumbar spine modifier and thoracic kyphosis [3–5]. The type 5 curve is defined as a structural thoracolumbar/lumbar curve, with nonstructural upper-thoracic and main-thoracic curves [3,5,6].

The corrective surgery with an anterior approach for thoracolumbar/lumbar curves was developed by Dwyer et al. in the 1970s [7]. Although the anterior approach remains useful for Lenke type 5 AIS, posterior spinal fusion with pedicle screw instrumentation

is currently the standard technique, with a relatively low complication rate [8–10]. Some authors have demonstrated that the posterior approach has no significant difference in the coronal and sagittal correction compared to the anterior approach, although the anterior approach has the advantage of saving fusion levels [11–15].

Although optimal rod contouring is essential for anatomical spinal correction, the rod contouring procedure highly depends on the surgeon's knowledge or experience [16]. Additionally, the notches generated in rod contouring decrease the mechanical properties of the rod [17,18]. We previously developed anatomically designed notch-free, pre-bent rods for patients with Lenke type 1 or 2 AIS, which resulted in reduced intraoperative rod deformation and improved thoracic kyphosis after the correction [16,19]. However, this implantation system is not applicable to Lenke type 5 AIS. This study aimed to determine the optimum rod geometries to provide a pre-bent rod system for posterior spinal surgery in patients with Lenke type 5 AIS by classifying the rod shape before implantation.

2. Materials and Methods

2.1. Patients

After institutional review board approval (approval number: 020-0416), we included 20 consecutive patients with Lenke type 5 AIS (2 men and 18 women) who underwent posterior spinal fusion between 2021 and 2023 at our institutions. Informed consent for this study and the publication of the information were obtained from all the participants and their guardians or parents, as applicable. Patients with syndromic, congenital, and neuromuscular scoliosis were excluded. Patients with Lenke types 1–4 and type 6 AIS curves were also excluded. The average age and body height at operation were 14.7 ± 1.9 years (range, 12–18) and 157.7 ± 6.6 cm (range, 149–173), respectively.

2.2. Radiographic Parameters

We investigated multiple parameters using a preoperative and 2-week follow-up standing long-cassette posteroanterior, lateral radiographs, and computed tomography (CT) [19]. The coronal measurements included the main thoracic curve angle, the thoracolumbar and lumbar curve angles, and L4 tilt. The global coronal balance was evaluated using the distance between the C7 plumb line and the center sacrum vertical line (C7–CSVL). The sagittal measurement included the thoracic kyphosis (T5–12) and lumbar lordosis (L1–S1). The sagittal balance was evaluated in the interval between the C7 plumb line and the S1 posterior superior corner (sagittal vertical axis). The vertebral rotation was measured using the axial plane of the CT image. In addition, the rod angles outlined below were also measured as indicators of rod deformation.

2.3. Rod Angle

The rod angle was measured using the rod shape on the left side. Prior to applying the contouring rod to the screw head, the contours of the rod shapes were traced on paper [16]. The angle between the proximal and distal tangential lines was measured at the proximal and distal curvature before implantation (θP1 and θD1, respectively) (Figure 1). The postoperative implant rod shape was obtained from the Digital Imaging and Communications in Medicine (DICOM) data from the 1-week postoperative CT scan. DICOM data were used to reconstruct the sagittal rod images using a DICOM viewer software (OsiriX Lite 12.0.1, Pixmeo Labs, Geneva, Switzerland). The postoperative rod angles were evaluated in a similar manner to that of the preoperative measurements from the sagittal reconstructed rod images (θP2 and θD2, respectively) (Figure 1). The difference between θ1 and θ2 (θ1–θ2) was calculated as the rod deformation ($\Delta\theta$) [20–22].
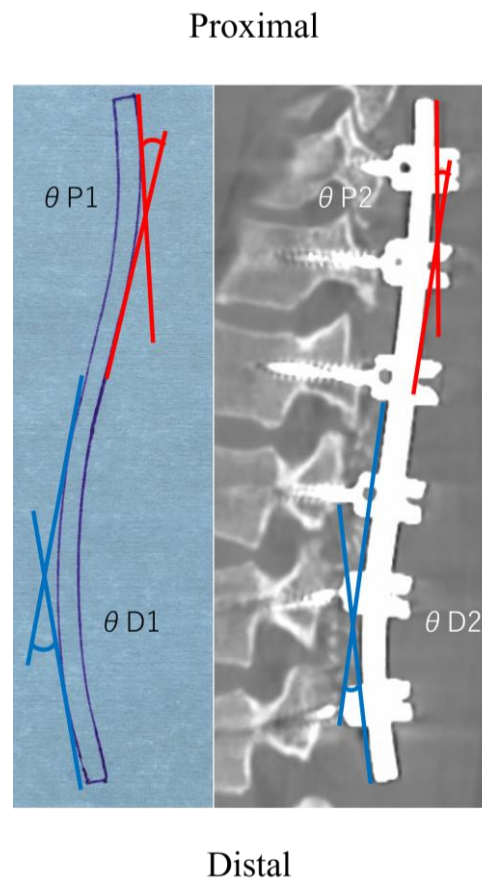
Proximal

Distal

Figure 1. Definition of pre- and postoperative rod angles.

2.4. Surgical Techniques

The correction surgery was performed using 5.5 mm diameter cobalt–chrome alloy implant rods and polyaxial pedicle screws (Continuously Variable Simulation SPINAL SYSTEM, ROBERT REID INC., Tokyo, Japan). We avoided implantation to L4, L5, and S1 as the lowest instrumented vertebra (LIV), considering the postoperative degenerative changes in the remaining mobile segments. The operative procedures, in brief, were as follows [16,19]: After the posterior spinal elements were exposed, the placement of the pedicle screw was performed with the resection of all-level facets within the instrumentation level. Both side rods were contoured to achieve the ideal postoperative coronal and sagittal alignments. After both side rods were applied to all screw heads, both side rods were simultaneously rotated. An in situ rod-bending maneuver to add to the correction was not performed.

2.5. Algorithm for Analyzing and Identifying the Optimal Rod Shapes

The optimal shapes for the pre-cut and pre-bent rods were found after performing the following steps.

Step 1: Generation of a center point cloud for existing rod shapes

First, papers with hand-traced outlines of 20 rods were scanned and converted into a JPEG file. Next, a computer-aided design (CAD) operator manually fit a sequence of circular arcs and straight lines to the outline images of each rod shape on an AutoCAD 2016 (Autodesk, Inc., San Rafael, CA, USA) and Solidworks (Dassault Systèmes SolidWorks Corp, Waltham, MA, USA). Subsequently, the sequence of circular arcs and straight lines of the rods' outlines were exported to an Excel file, and a center point cloud, P_i, of a rod $i \in R(R = \{1, 2, \ldots, 20\}$: a set of all rods), was generated by deriving the center curves of the input arcs and lines and by taking the constant-length sampling of the center curves

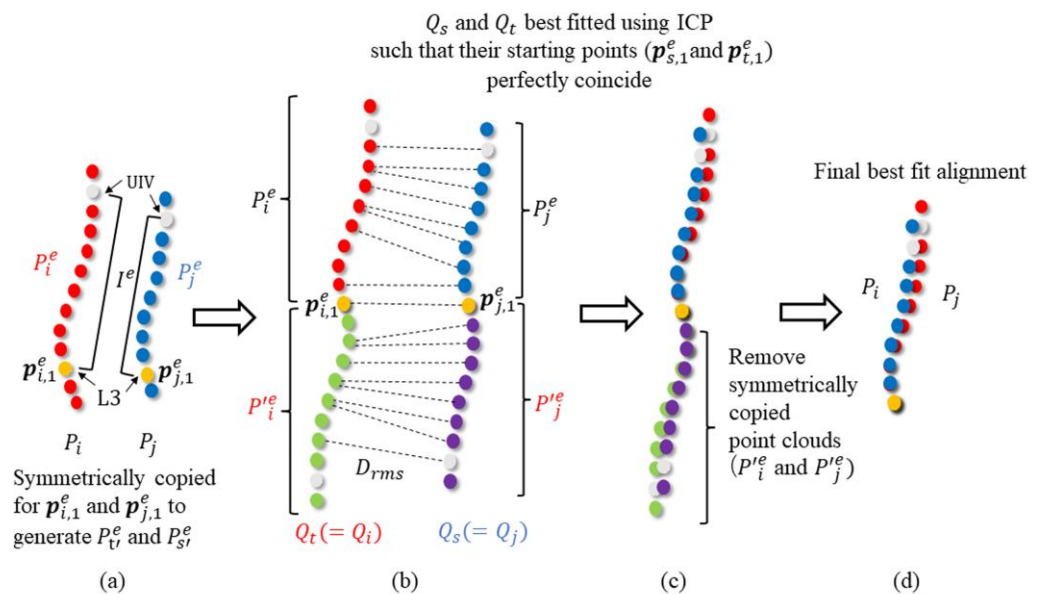using our original MATLAB (MATLAB R2022b for Windows: The Mathworks, Natick, MA, USA) code (Figure 2a).

Figure 2. Evaluation of the difference between rods using the modified iterative closest point (ICP) method. (**a**) The center points of rods i and j that are included in the evaluation interval I^e (from the UIV to L3) are selected as P_i^e and P_j^e from the original center point clouds P_i and P_j. The points closest to the fixation point of L3 in P_i^e and P_j^e are selected as their starting points, $p_{i,1}^e$ and $p_{j,1}^e$, respectively. (**b**) The points P_i^e and P_j^e are symmetrically copied with respect to their starting points $p_{i,1}^e$ and $p_{j,1}^e$. Then, P_i^e and P_j^e and their symmetrically copied points $P_i'^e$ and $P_j'^e$ are combined as Q_i and Q_j. Of the two point clouds Q_i and Q_j, the one with the longer length is selected as the target point cloud Q_t, and the other as the source point cloud Q_s. (**c**) The source point cloud Q_s is best fitted to the target point cloud Q_t using the ICP method. (**d**) The final best-fit alignment between point clouds P_i and P_j was obtained by removing $P_i'^e$ and $P_j'^e$ from Q_s and Q_t at their best-fit position.

Step 2: Hierarchical cluster analysis for length-based grouping of the existing rods

Since the curve lengths of the center point clouds of the 20 rods ranged from 145 to 220 mm, knowing which rods could be aggregated into one group based on length criteria was essential to prepare for the rod pre-cutting process. To this end, the difference in curve lengths between all the rods was evaluated as the distance between the different rods first, and a hierarchical cluster analysis with a complete linkage was conducted for the balanced, length-based grouping of the rods using our MATLAB code. The cluster analysis can identify the rod groups $G_1, G_2, \ldots, G_j, \ldots, G_K$, $(G_j \subseteq R, K$: the total number of rod groups) such that the maximum difference in length among the rods in a group G_j is less than the allowable value.

Step 3: Evaluation of geometric difference among rods using a modified iterative closest point (ICP) method

Because the initial positions and orientations of the center point clouds of the rods $\{P_I\}$ in rod group G_k are not necessarily aligned, the center point clouds in G_k were first best fitted to each other using our modified ICP [23] method before evaluating the difference in curve geometry among the rod shapes in G_k. As shown in Figure 2a, a subset of the center point clouds that were included only in the evaluation interval I^e from the upper instrumented vertebra (UIV) to L3 were selected as targets of the alignment using the modified ICP, because L3 was fixed as the LIV. The center points included in the evaluation interval I_i^e of a rod i were extracted from an original center point cloud I, which was defined as an evaluation point cloud P_i^e.

As shown in Figure 2b, in the point cloud alignment using the modified ICP, first, a point $I_{i,1}^e (\in P_i^e)$, closest to the fixation point of L3 was selected as the starting point for the evaluation of point cloud P_i^e. Then, all the other points in P_i^e were point-symmetrically copied with respect to I, and the union of the original points P_i^e and their copied points $P_i'^e$ was created as the combined point cloud $Q_i (= P_i^e \cup P_i'^e)$. This copy and union process was performed for the evaluation of point cloud P_i^e for all the rods.

As shown in Figure 2b, when aligning two combined point clouds Q_i and Q_j in a rod group G_k, the point cloud with the shorter evaluation interval length was selected as the source point cloud Q_s, and the point cloud with the longer interval length was chosen as target point cloud Q_t. Subsequently, the source point cloud Q_s was best fitted to the target point cloud Q_t using the following ICP method [23].

For the point cloud alignment using ICP, first, for all points $p_{s,m}$ in Q_s, the point $p_{t,c(m)}$ closest to $p_{s,m}$ is searched for in Q_t, where $c(m)$ denotes the index of the point in Q_t that is closest to $p_{s,m}$ in Q_s. Next, the optimum position and orientation $\langle R', t' \rangle$ for Q_s that best fits Q_s to Q_t can be found by solving the following Equations (1) and (2), where the mean square distance D_{rms}^2 between the closest point pairs $(p_{s,m}, p_{t,c(m)})$ is minimized [16].

$$\langle R', t' \rangle = \underset{\langle R,t \rangle}{\arg\min} \, D_{rms}^2 \tag{1}$$

$$D_{rms} = \sqrt{\frac{1}{|Q_s|} \sum_{p_{s,m} \in Q_s} \left\| R p_{s,m} + t - p_{t,c(m)} \right\|^2} \tag{2}$$

where R denotes a 3×3 rotation matrix, t denotes a translation vector for transforming the source point cloud Q_S, and $|Q_S|$ refers to the number of points in Q_S.

After that, every point $p_{s,m}$ in Q_S is repositioned into its optimum position and orientation by applying $\langle R', t' \rangle$ to $p_{s,m}$ as defined in Equation (3):

$$p_{s,m} \leftarrow R' p_{s,m} + t' \tag{3}$$

The derivation of the best-fit transformation for Q_S using Equations (1) and (2) and the transformation of Q_S using Equation (3) are repeated until the rotation and translation $\langle R', t' \rangle$ converge and, as a result, the final best-fit position and orientation of Q_S to Q_t is derived.

It is guaranteed that the centroids of Q_S and Q_t theoretically coincide in the best fit of Q_S to Q_t using the ICP, and the centroids of Q_S and Q_t are their starting points $p_{s,1}^e$ and $p_{t,1}^e$, respectively. Therefore, as shown in Figure 2c, the best-fit alignment of Q_S and Q_t can be obtained, such that both starting points $p_{s,1}^e$ and $p_{t,1}^e$ that are closest to the fixation points of L3 coincide with each other [23]. Finally, as shown in Figure 2d, the symmetrically copied points $P_s'^e$ and $P_t'^e$ are removed from Q_s and Q_t to obtain the final best-fit alignment of the center point clouds P_s and P_t of two different rods s and t in a rod group.

Step 4: Evaluation of rod shape difference

If the maximum gap between one rod shape and the other is large, the created pre-bent rod may not be applied to the screw head during the corrective surgery. To this end, the maximum difference between rods i and j was evaluated as the maximum distance between their center point clouds, P_i and P_j, under their best-fit aligned position as follows: The point clouds in a given a point cloud P_i were first transformed into their best-fit position P_j using the best-fit rotation R^* and translation t^* already derived from step 3. The maximum distance D_{max} between point clouds P_i and P_j was evaluated as per Equation (4):

$$D_{max} = \underset{p_{i,m} \in P_i}{\max} \left\{ \left\| R^* p_{i,m} + t^* - p_{j,d(m)} \right\| \right\} \tag{4}$$

where $p_{j,d(m)}$ is the point in P_j that is closest to $R^* p_{i,m} + t^*$.

This D_{max} was used as an indicator of the difficulty of rod application during corrective surgery [16,23].

However, since D_{rms} at the best-fitted alignment, as defined in Equation (2), represents the overall similarity in shape between center point clouds P_i and P_j, the hierarchical cluster analysis in the following step was conducted using D_{rms} as the distance to evaluate the similarity in shape between rods i and j in a rod group G_j.

Step 5: Hierarchical cluster analysis among rod shapes

Since the rod groups $G_1, G_2, \ldots, G_j, \ldots, G_K$ were created based only on the similarity in rod length, various rod shapes might be included within a single group. Therefore, to assess the similarity in rod shapes in a rod group G_j, and identify the subgroups with similar rod shapes $H_{j1}, H_{j2}, \cdots, H_{jL}, \left(G_j = \bigcup_{k \in [1,L]} H_{jk} \right)$ in a given rod group G_j, a hierarchical cluster analysis was conducted using the criteria of complete linkage. D_{rms} was adopted as the distance between two rod shapes in the cluster analysis [16,23]. The maximum allowable distance for D_{rms} within a cluster of a subgroup H_{jk} was determined as 5 mm according to a previous study [16]. The cluster analysis revealed a subgroup of rods with similar rod geometry and rod length.

Step 6: Derivation of a pre-bent and pre-cut rod shape from the representative curve in rod subgroups

Finally, for each subgroup of rods with a similar length and shape, H_{jk}, found in Step 5, a representative curve that best fits them was generated, and then a 3D model of the pre-bent and pre-cut rod shape was derived, whose center curve was identical to the representative curve.

Since all the center points of the rods $\left\{ P_i \middle| i \in H_{jk} \right\}$ were best fitted to each other in a subgroup H_{jk} using ICP similar to that in step 3, a union of the best-fitted center points $P_{jk}^U = \bigcup_{i \in H_{jk}} P_i$ was first created for the subgroup H_{jk}. Next, a smooth B-spline curve C_{jk}^U was best fitted to all the center points included in P_{jk}^U using the iterative least-square fitting method [16,23]. Because the best-fit curve C_{jk}^U can be regarded as the curve representative of the center curve shapes of all the rods included in the subgroup H_{jk}, the curve C_{jk}^U can be used as the center curve of the pre-bent and pre-cut rod shape for the rod subgroup H_{jk} [16,23]. Therefore, the triangle mesh for a pre-bent and pre-cut rod shape was generated by sweeping a circle with a user-defined rod diameter along the B-spline curve C_{jk}^U of the subgroup H_{jk}. Finally, the pre-bent and pre-cut rod shapes represented by the triangle meshes were saved as a standard triangulated language (STL) file.

3. Results

The patients' demographic data are summarized in Table 1. Although the preoperative thoracolumbar/lumbar curve was 42.2°, the postoperative radiographs show an improvement to a thoracolumbar/lumbar curve of 5.9°. The sagittal plane analysis revealed that the preoperative lumbar lordosis was 46.4°, which increased significantly to 50.6° ($p = 0.04$). The preoperative and postoperative implant rod angles are listed in Table 2. The UIV was selected as T9 in seven patients, T10 in 11 patients, and T11 in two patients, whereas the LIV was L3 in all the patients. The proximal rod angle changed from an θP1 of 18.3° to an θP2 of 9.3°, and the distal rod angle changed from an θD1 of 30.8° to an θD2 of 15.9°, indicating that both the proximal and distal rod angles significantly decreased after the correction. There was no correlation between the change in rod angle and any of the radiographic parameters (Table 2).

Table 1. Patients' pre- and postoperative demographic data.

Radiographic Parameter	Pre-Operative	Postoperative	*p* Value
Thoracolumbar/lumbar curve (°)	42.2 ± 6.6	5.9 ± 2.4	<0.01
Thoracic curve (°)	22.0 ± 8.5	11.9 ± 8.0	<0.01
L4 tilt (°)	20.7 ± 4.3	6.7 ± 3.2	<0.01
Thoracic kyphosis (T5-12) (°)	24.9 ± 11.1	29.8 ± 8.0	0.02
Lumbar lordosis (L1-S1) (°)	46.4 ± 14.5	50.6 ± 12.2	0.04
C7 translation from CSVL (mm)	24.7 ± 14.6	16.9 ± 10.1	0.05
Apical vertebral translation (mm)	43.1 ± 9.3	8.9 ± 4.3	<0.01
Sagittal vertical axis (mm)	-0.4 ± 28.6	5.5 ± 25.2	0.34
Vertebral rotation (°)	20.3 ± 10.8	12.4 ± 5.0	<0.01
Proximal rod angle (°)	18.3 ± 6.7	9.3 ± 3.3	<0.01
Distal rod angle (°)	30.8 ± 8.0	15.9 ± 4.6	<0.01

Table 2. Correlation between rod deformation and radiographic parameters.

Variable	Rod Deformation ($\Delta\theta P$) Correlation Coefficient	Statistical Significance	Rod Deformation ($\Delta\theta D$) Correlation Coefficient	Statistical Significance
Postoperative main Cobb angle	$r = 0.07$	$p = 0.76$	$r = 0.29$	$p = 0.18$
Change in main Cobb angle	$r = -0.20$	$p = 0.37$	$r = 0.01$	$p = 0.96$
Postoperative L4 tilt	$r = 0.03$	$p = 0.88$	$r = 0.25$	$p = 0.25$
Change in L4 tilt	$r = -0.10$	$p = 0.65$	$r = 0.11$	$p = 0.61$
Postoperative lumbar lordosis	$r = 0.21$	$p = 0.35$	$r = 0.01$	$p = 0.95$
Change in lumbar lordosis	$r = 0.30$	$p = 0.17$	$r = -0.36$	$p = 0.10$
Postoperative thoracic kyphosis	$r = 0.15$	$p = 0.50$	$r = 0.18$	$p = 0.43$
Change in thoracic kyphosis	$r = 0.22$	$p = 0.32$	$r = -0.23$	$p = 0.31$

The rods were classified into four clusters according to their length (Figure 3). The number of rods was two in cluster 1 (140–150 mm), eleven in cluster 2 (165–190 mm), five in cluster 3 (195–205 mm), and two in cluster 4 (210–225 mm). The dendrogram obtained using the ICP method is shown in Figure 4. Without dividing the point clouds in the length-based cluster, the D_{rms}, which is the overall difference between each point cloud, was <5 mm in all the clusters (Table 3). The D_{rms} and the D_{max} between the best-fitted curvature and the other point clouds of the rods in each cluster are shown in Table 3. The D_{rms} ranged from 0.21 to 1.91 mm, and the D_{max} ranged from 0.46 to 4.32 mm. Finally, the best-fitted curvature and STL images for the three-dimensional rods in each cluster are presented in Figure 5.
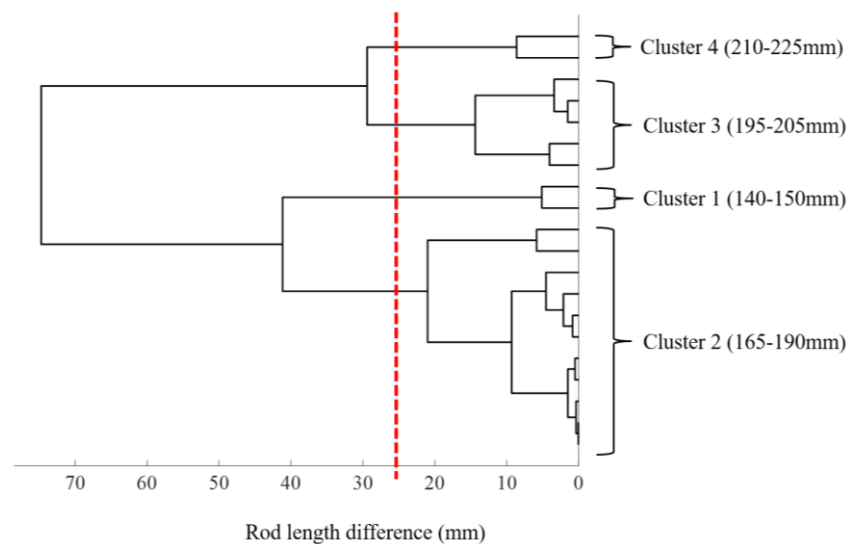

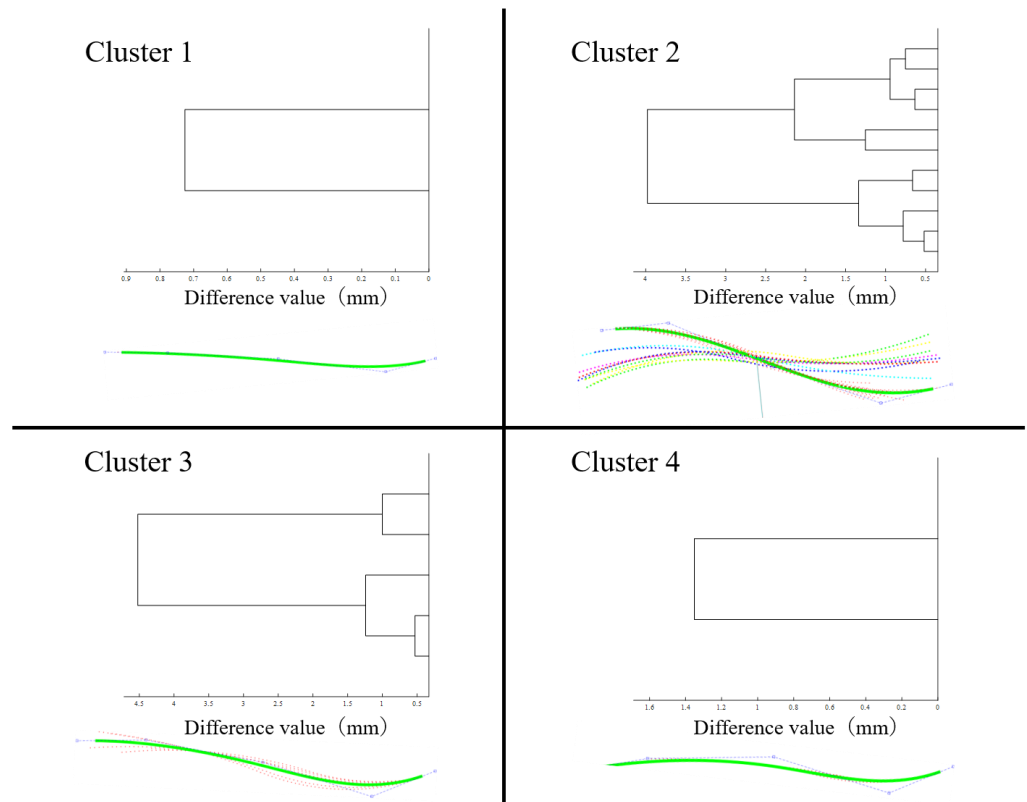**Figure 3.** Hierarchical cluster analysis based on rod length.

Figure 4. Dendrogram and best-fitted curves in each cluster obtained using the iterative closest point method.

Table 3. The value of D_{rms} and D_{max} in each comparison.

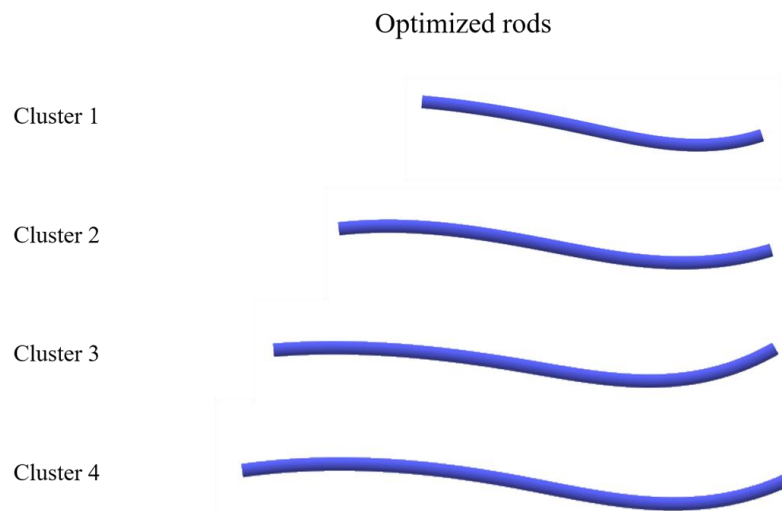|	The Value between Each Point Cloud		The Value between Best-Fitted Curvature and the Other Point Clouds	
	D_{rms}	D_{max}	D_{rms}	D_{max}
Cluster 1	0.72	0.99	0.21	0.46
Cluster 2	3.98	8.35	1.18	4.32
Cluster 3	4.52	8.78	1.91	4.67
Cluster 4	1.35	2.19	0.57	1.16

Figure 5. Standard triangulated language (STL) images of the optimized rod.

4. Discussion

The ICP method with modification was applied for identifying the optimal rod shape for the Lenke type 5 curve in this study. Our algorithm is modified at the point of best fitting between two rods at the target point, by making symmetrically copied points from the target point as compared to the ICP method used in previous studies [16,24], so that the fixation points on two rods that are the target points of the evaluation intervals are perfectly matched.

In the present study, in the cluster analysis for length classification, 20 rods were di-vided into four clusters with intervals of <25 mm. The D_{rms} was within 5 mm in each rod length-based cluster, indicating that it was possible for the point clouds for rod shape to converge to one best-fitted curve in each length-based cluster, because the thoracic pre-bent rod was created based on a $D_{rms} < 5$ mm in each cluster in a previous study [16]. Furthermore, the maximum D_{rms} and D_{max} between the best-fitted B-spline curvature and the other point clouds in each cluster were 1.9 and 4.7 mm, respectively, whereas the thoracic best-fitted curvature in a previous study had a D_{rms} of 2.2 mm and a D_{max} of 6.0 mm [16]. These thoracic pre-bent rods resulted in a good sagittal alignment in the correction of 27 patients with a Lenke type 1 curve without additional rod bending, suggesting that the four preset rod shapes with best-fitted B-spline curvature can be applied to the correction of patients with a Lenke type 5 curve without additional rod bending [19].

Considering mechanical implant failure and correction loss, the material and fatigue life of rods are also essential in developing a pre-bent rod [25]. Some authors [26–30] have described that cobalt–chromium alloy rods had a significantly higher stiffness than titanium alloy rods. In the current study, the rod angle of the convex side significantly decreased the proximal and distal curvature in the contoured rods, whereas the rod deformation did not affect the postoperative coronal and sagittal alignment parameters and changes. Although all the correction surgeries were performed using cobalt–chromium alloy rods, the titanium alloy rod can have a larger rod deformation that can influence postoperative outcomes. Furthermore, despite performing rod contouring prior to implantation in this series, the notch created by intraoperative bending should be avoided from the viewpoint of its impact on the postoperative coronal and sagittal outcomes due to rod deformation [31]. Notch-free cobalt–chromium alloy rods are optimum for the correction surgery for patients with Lenke type 5 curves to prevent rod deformation and obtain excellent radiographic parameters.

The twenty patients in this study showed improvements of 42.2° to 5.9° in the thoracolumbar/lumbar curve, 22.0° to 11.9° in the thoracic curve, and 20.7° to 6.7° in the L4 tilt. Additionally, thoracic kyphosis and lumbar lordosis were maintained as having good sagittal alignment. These postoperative outcomes will be promised in the correction surgery for Lenke type 5 AIS if using the presented four pre-bent rods. Moreover, these pre-bent rods not only provide good corrective outcomes but could also be useful in reducing the burden on patients and the surgeon in AIS correction. Although rod contouring depends on the surgeon's experience or intuition, a mismatched rod configuration can lead to an incomplete correction and difficulty when applying the screws, which can increase anesthesia time and excessive bleeding. Some articles [32–35] have reported that using patient-specific pre-bent rods reduced the operating time for deformity corrections without rod contouring during surgery. The four preset rods will benefit patients and surgeons by shortening the operating time or by eliminating the dependence of the technique on the surgeon.

This study has some limitations. First, the four representative rod shapes for Lenke type 5 AIS were identified using traced rod shape data for 20 patients, meaning that the rod shape for Lenke type 5 was aggregated by one-fifth; however, it is unclear whether 20 cases are sufficient to create pre-bent rods for Lenke type 5 AIS correction. Nevertheless, clusters 1 and 2, with only two point clouds, would maintain the D_{rms} within 5 mm even if the number of point clouds in these clusters increased, because the D_{rms} of cluster 2, which has a maximum point cloud number of 11, was 4.0 mm. Second, these four rods can only be adopted for the correction of a thoracolumbar/lumbar curve with an LIV of L3, because

L3 was selected as the LIV for all the cases in this study. We avoided selecting L4 or the vertebrae caudal to L4 as the LIV so as to not progress degenerative change by diminishing spinal mobile segments. However, it remains controversial whether to include L4 as the LIV in the correction of the thoracolumbar/lumbar curve, despite L4 being selected as the LIV by surgeons to prevent the risk of decompensation, especially for the large and rigid thoracolumbar/lumbar curve [36–38]. However, our algorithm used to develop the pre-bent rods is available to create the pre-bent rod for an LIV of L4 if there are rod shape data. Finally, the outcomes in the present study are based on 2-week follow-up radiographs and a 1-week-postoperative CT scan. Because the long-term clinical outcomes of the 20 patients in this study are unknown, the long-term outcomes of correction using these pre-bent rods should be validated. However, Yamada et al. [39] reported a good correction rate for Lenke type 5 posterior surgery, which was performed using the same surgical technique as in this study with manually bent rods, both immediately postoperative and 2 years after the operation.

5. Conclusions

We identified four optimum rod shapes (one-fifth of the total) from 20 patients to develop pre-bent rods designed for corrective surgery for thoracolumbar/lumbar adolescent idiopathic scoliosis. These pre-bent rods will be beneficial in achieving proper postoperative outcomes without rod contouring based on surgeon experience. They will also contribute to reducing the patients' burden by diminishing operation time and blood loss.

Author Contributions: Conceptualization, H.S. (Hideki Sudo); methodology, Y.I., S.K., K.U., T.K. and H.S. (Hideki Sudo); software, S.K. and H.S. (Hideki Sudo); validation, Y.I., T.K. and H.S. (Hideki Sudo); formal analysis, Y.I., S.K., T.K. and H.S. (Hideki Sudo); investigation, Y.I., S.K., K.U., T.K., K.Y., Y.A., H.T., H.S. (Hisataka Suzuki), T.O., T.E., D.U., M.T. and H.S. (Hideki Sudo); resources, S.K. and H.S. (Hideki Sudo); data curation, Y.I., S.K., T.K. and H.S. (Hideki Sudo); writing—original draft preparation, Y.I., S.K., T.K. and H.S. (Hideki Sudo); writing—review and editing, H.S. (Hideki Sudo); visualization, Y.I., S.K., T.K. and H.S. (Hideki Sudo); supervision, N.I.; project administration, H.S. (Hideki Sudo); funding acquisition, H.S. (Hideki Sudo). All authors have read and agreed to the published version of the manuscript.

Institutional Review Board Statement: The study was conducted in accordance with the Declaration of Helsinki and approved by the Institutional Review Board of Hokkaido University Hospital (approval number: 020-0416).

Informed Consent Statement: Informed consent was obtained from all the subjects involved in this study.

Data Availability Statement: The data that support the findings of this study are available from the corresponding author on reasonable request.

Conflicts of Interest: The authors declare no conflict of interest.

References

1. Altaf, F.; Gibson, A.; Dannawi, Z.; Noordeen, H. Adolescent idiopathic scoliosis. *BMJ* **2013**, *346*, f2508. [CrossRef] [PubMed]
2. Addai, D.; Zarkos, J.; Bowey, A.J. Current concepts in the diagnosis and management of adolescent idiopathic scoliosis. *Child's Nerv. Syst.* **2020**, *36*, 1111–1119. [CrossRef] [PubMed]
3. Lenke, L.G.; Betz, R.R.; Harms, J.; Bridwell, K.H.; Clements, D.H.; Lowe, T.G.; Blanke, K. Adolescent idiopathic scoliosis: A new classification to determine extent of spinal arthrodesis. *J. Bone Joint Surg. Am.* **2001**, *83*, 1169–1181. [CrossRef] [PubMed]
4. Hosseinpour-Feizi, H.; Soleimanpour, J.; Sales, J.G.; Arzroumchilar, A. Lenke and King classification systems for adolescent idiopathic scoliosis: Interobserver agreement and postoperative results. *Int. J. Gen. Med.* **2011**, *4*, 821–825. [CrossRef]
5. Ovadia, D. Classification of adolescent idiopathic scoliosis (AIS). *J. Child. Orthop.* **2013**, *7*, 25–28. [CrossRef]
6. Lenke, L.G.; Betz, R.R.; Clements, D.; Merola, A.; Haher, T.; Lowe, T.; Newton, P.; Bridwell, K.H.; Blanke, K. Curve prevalence of a new classification of operative adolescent idiopathic scoliosis: Does classification correlate with treatment? *Spine* **2002**, *27*, 604–611. [CrossRef]

7.   Helenius, I. Anterior surgery for adolescent idiopathic scoliosis. *J. Child. Orthop* **2013**, *7*, 63–68. [CrossRef]
8.   Chen, Z.; Rong, L. Comparison of combined anterior-posterior approach versus posterior-only approach in treating adolescent idiopathic scoliosis: A meta-analysis. *Eur. Spine J.* **2016**, *25*, 363–371. [CrossRef]
9.   Abel, M.F.; Singla, A.; Feger, M.A.; Sauer, L.D.; Novicoff, W. Surgical treatment of Lenke 5 adolescent idiopathic scoliosis: Comparison of anterior vs posterior approach. *World J. Orthop.* **2016**, *7*, 553–560. [CrossRef]
10.   O'Donnell, C.; Michael, N.; Pan, X.; Emans, J.; Garg, S.; Erickson, M. Anterior Spinal Fusion and Posterior Spinal Fusion Both Effectively Treat Lenke Type 5 Curves in Adolescent Idiopathic Scoliosis: A Multicenter Study. *Spine Deform.* **2018**, *6*, 231–240. [CrossRef]
11.   Hirase, T.; Ling, J.F.; Haghshenas, V.; Thirumavalavan, J.; Dong, D.; Hanson, D.S.; Marco, R.A.W. Anterior versus posterior spinal fusion for Lenke type 5 adolescent idiopathic scoliosis: A systematic review and meta-analysis of comparative studies. *Spine Deform.* **2022**, *10*, 267–281. [CrossRef]
12.   Wang, Z.W.; Shen, Y.Q.; Wu, Y.; Li, J.; Liu, Z.; Xu, J.K.; Chen, Q.X.; Chen, W.S.; Chen, L.W.; Zhang, N.; et al. Anterior Selective Lumbar Fusion Saving More Distal Fusion Segments Compared with Posterior Approach in the Treatment of Adolescent Idiopathic Scoliosis with Lenke Type 5: A Cohort Study with More Than 8-Year Follow-up. *Orthop. Surg.* **2021**, *13*, 2327–2334. [CrossRef] [PubMed]
13.   Luo, M.; Wang, W.; Shen, M.; Xia, L. Anterior versus posterior approach in Lenke 5C adolescent idiopathic scoliosis: A meta-analysis of fusion segments and radiological outcomes. *J. Orthop. Surg. Res.* **2016**, *11*, 77. [CrossRef] [PubMed]
14.   Liang, W.; Han, B.; Sun, D.; Hai, Y.; Yin, P.; Liu, Y.; Yang, J. Surgical Treatment of Scoliosis Lenke Type 5, Anterior Versus Posterior, Which Approach is Better?: A Systematic Review and Meta-Analysis. *Spine* **2023**, *48*, E223–E234. [CrossRef] [PubMed]
15.   Yoshihara, H. Surgical Treatment of Lenke Type 5 Adolescent Idiopathic Scoliosis: A Systematic Review. *Spine* **2019**, *44*, E788–E799. [CrossRef]
16.   Kokabu, T.; Kanai, S.; Abe, Y.; Iwasaki, N.; Sudo, H. Identification of optimized rod shapes to guide anatomical spinal reconstruction for adolescent thoracic idiopathic scoliosis. *J. Orthop. Res.* **2018**, *36*, 3219–3224. [CrossRef]
17.   Lindsey, C.; Deviren, V.; Xu, Z.; Yeh, R.F.; Puttlitz, C.M. The effects of rod contouring on spinal construct fatigue strength. *Spine* **2006**, *31*, 1680–1687. [CrossRef]
18.   Ferrero, E.; Mazda, K.; Simon, A.L.; Ilharreborde, B. Preliminary experience with SpineEOS, a new software for 3D planning in AIS surgery. *Eur. Spine J.* **2018**, *27*, 2165–2174. [CrossRef]
19.   Sudo, H.; Tachi, H.; Kokabu, T.; Yamada, K.; Iwata, A.; Endo, T.; Takahata, M.; Abe, Y.; Iwasaki, N. In vivo deformation of anatomically pre-bent rods in thoracic adolescent idiopathic scoliosis. *Sci. Rep.* **2021**, *11*, 12622. [CrossRef]
20.   Seki, S.; Newton, P.O.; Yahara, Y.; Makino, H.; Nakano, M.; Hirano, N.; Kawaguchi, Y.; Kimura, T. Differential Rod Contouring is Essential for Improving Vertebral Rotation in Patients with Adolescent Idiopathic Scoliosis: Thoracic Curves Assessed with Intraoperative CT. *Spine* **2018**, *43*, E585–E591. [CrossRef]
21.   Cidambi, K.R.; Glaser, D.A.; Bastrom, T.P.; Nunn, T.N.; Ono, T.; Newton, P.O. Postoperative changes in spinal rod contour in adolescent idiopathic scoliosis: An in vivo deformation study. *Spine* **2012**, *37*, 1566–1572. [CrossRef] [PubMed]
22.   Salmingo, R.; Tadano, S.; Fujisaki, K.; Abe, Y.; Ito, M. Corrective force analysis for scoliosis from implant rod deformation. *Clin. Biomech.* **2012**, *27*, 545–550. [CrossRef] [PubMed]
23.   Soutome, A.; Kanai, S.; Date, H.; Kokabu, T.; Abe, Y.; Moridaira, H.; Taneichi, H.; Sudo, H. Preliminary Shape Similarity Analysis and Standardization for Pre-Bent Rod Design for Adult Spinal Deformity Correction. *Comput. Aided Des. Appl.* **2023**, *20*, 797–813. [CrossRef]
24.   Besl, P.J.; McKay, H.D. A method for registration of 3-D shapes. *IEEE Trans. Pattern Anal. Mach. Intell.* **1992**, *1611*, 586–606. [CrossRef]
25.   Bowden, D.; Michielli, A.; Merrill, M.; Will, S. Systematic review and meta-analysis for the impact of rod materials and sizes in the surgical treatment of adolescent idiopathic scoliosis. *Spine Deform.* **2022**, *10*, 1245–1263. [CrossRef]
26.   Lee, Y.; Welsch, G. Young's modulus and damping of Ti 6Al 4 Valloy as a function of heat treatment and oxygen concentration. *Mater. Sci. Eng. A Struct. Mater.* **1990**, *128*, 77–89. [CrossRef]
27.   Fan, Z. On the young's moduli of Ti 6Al 4V alloys. *Scr. Metall. Mater.* **1993**, *29*, 1427–1432. [CrossRef]
28.   Sabah, Y.; Clément, J.L.; Solla, F.; Rosello, O.; Rampal, V. Cobalt-chrome and titanium alloy rods provide similar coronal and sagittal correction in adolescent idiopathic scoliosis. *Orthop. Traumatol. Surg. Res.* **2018**, *104*, 1073–1077. [CrossRef]
29.   Staiger, M.P.; Pietak, A.M.; Huadmai, J.; Dias, G. Magnesium and its alloys as orthopedic biomaterials: A review. *J. Biomater.* **2006**, *27*, 1728–1734. [CrossRef]
30.   Nguyen, T.Q.; Buckley, J.M.; Ames, C.; Deviren, V. The fatigue life of contoured cobalt chrome posterior spinal fusion rods. *Proc. Inst. Mech. Eng. H* **2011**, *225*, 194–198. [CrossRef]
31.   Demura, S.; Murakami, H.; Hayashi, H.; Kato, S.; Yoshioka, K.; Yokogawa, N.; Ishii, T.; Igarashi, T.; Fang, X.; Tsuchiya, H. Influence of Rod Contouring on Rod Strength and Stiffness in Spine Surgery. *Orthopedics* **2015**, *38*, e520-3. [CrossRef]
32.   Solla, F.; Barrey, C.Y.; Burger, E.; Kleck, C.J.; Fière, V. Patient-specific Rods for Surgical Correction of Sagittal Imbalance in Adults: Technical Aspects and Preliminary Results. *Clin. Spine Surg.* **2019**, *32*, 80–86. [CrossRef] [PubMed]
33.   Solla, F.; Clément, J.L.; Cunin, V.; Bertoncelli, C.M.; Fière, V.; Rampal, V. Patient-specific rods for thoracic kyphosis correction in adolescent idiopathic scoliosis surgery: Preliminary results. *Orthop. Traumatol. Surg. Res.* **2020**, *106*, 159–165. [CrossRef] [PubMed]

34. Prost, S.; Farah, K.; Pesenti, S.; Tropiano, P.; Fuentes, S.; Blondel, B. "Patient-specific" rods in the management of adult spinal deformity. One-year radiographic results of a prospective study about 86 patients. *Neurochirurgie* **2020**, *66*, 162–167. [CrossRef]

35. Barton, C.; Noshchenko, A.; Patel, V.; Kleck, C.; Burger, E. Early Experience and Initial Outcomes with Patient-Specific Spine Rods for Adult Spinal Deformity. *Orthopedics* **2016**, *39*, 79–86. [CrossRef] [PubMed]

36. Qin, X.; He, Z.; Yin, R.; Qiu, Y.; Zhu, Z. Where to stop distally in Lenke modifier C AIS with lumbar curve more than 60°: L3 or L4? *Clin. Neurol. Neurosurg.* **2019**, *178*, 77–81. [CrossRef]

37. LaValva, S.M.; Anari, J.B.; Flynn, J.M. Risk factors for persistent coronal imbalance or revision surgery following L3 LIV selection in adolescent idiopathic scoliosis (AIS). *Spine Deform.* **2021**, *9*, 1063–1072. [CrossRef]

38. Chang, D.G.; Suk, S.I.; Song, K.S.; Kim, Y.H.; Oh, I.S.; Kim, S.I.; Park, H.Y.; Kim, G.U.; Lee, J.W.; Park, J.B.; et al. How to Avoid Distal Adding-on Phenomenon for Rigid Curves in Major Thoracolumbar and Lumbar Adolescent Idiopathic Scoliosis? Identifying the Incidence of Distal Adding-on by Selection of Lowest Instrumented Vertebra. *World Neurosurg.* **2019**, *132*, e472–e478. [CrossRef]

39. Yamada, K.; Sudo, H.; Abe, Y.; Kokabu, T.; Tachi, H.; Endo, T.; Ohnishi, T.; Ukeba, D.; Ura, K.; Takahata, M.; et al. Influence of Lateral Translation of Lowest Instrumented Vertebra on L4 Tilt and Coronal Balance for Thoracolumbar and Lumbar Curves in Adolescent Idiopathic Scoliosis. *J. Clin. Med.* **2023**, *12*, 1389. [CrossRef]